September 2025 Vol. 36 No. 3: 179-190

Organic matter burial and deposition conditions in the northern part of Chukchi Shelf, Arctic Ocean, since the Little Ice Age

YU Xiaoguo^{1,2*}, YE Liming^{1,2}, ZHANG Weiyan^{1,2*}, WANG Rong^{1,2}, BIAN Yeping^{1,2}, JIN Xiaobing^{1,2}, YAO Xuying^{1,2} & QIAN Jingxin^{1,2}

Received 4 April 2025; accepted 16 August 2025; published online 30 September 2025

Abstract Understanding the sediment record during the Little Ice Age (LIA) can help elucidate natural sea ice fluctuation and carbon cycle variability. This study analyzed the grain size composition (including ice-rafted debris), total organic carbon (TOC), total nitrogen (TN) content, and stable isotopic composition (δ^{13} C and δ^{15} N) of the sediment record (approximately 490 a) of core ARC7-R11 in the northern part of the Chukchi Shelf. The sediment grains comprise mostly (>90%) silt and clay components. The grain size composition suggests generally low-energy hydrodynamic conditions across the region, yet reveals a trend of enhancement in hydrodynamics from the bottom to top layers of the sediment core, particularly after the 1940s. It also shows occurrences of seasonal sea ice and retreat of the perennial sea ice margin during warmer periods of the LIA and the post-LIA period. The organic matter content is high throughout the core, with heavier δ^{13} C values and moderate TOC/TN ratios indicating primarily marine origin; the terrestrial input is <37.5% according to the endmember model. The variation trend of marine-derived organic carbon (OC) content is similar to that of summer temperature anomalies; while variation trend of terrestrially derived OC shows significant correlation with that of the number of ice-free days in the southern shelf region, except for the period from approximately 1700s to the 1870s. During the LIA, the TOC content fluctuated and decreased, and the relative contribution of terrestrial OC was higher than during the modern warm period. The amount of OC buried in the sediment has increased with climate warming, especially after the 1940s, reflecting the enhanced ability of sediment to sequester carbon during warmer periods.

Keywords grain size composition, ice-rafted debris, organic matter, northern Chukchi Shelf, Little Ice Age

Citation: Yu X G, Ye L M, Zhang W Y, et al. Organic matter burial and deposition conditions in the northern part of Chukchi Shelf, Arctic Ocean, since the Little Ice Age. Adv Polar Sci, 2025, 36(3): 179-190, doi: 10.12429/j.advps.2025.0005

1 Introduction

The Chukchi Shelf of the western Arctic Ocean (Figure 1) is known to be highly sensitive to climate variability (Bader et al., 2011; Danielson et al., 2014; Woodgate et al., 2010). In response to global warming, sea ice in the area

has diminished radically in terms of its concentration, volume, and persistence, while regional coastal erosion, permafrost thaw, fluvial sediment discharge, and terrestrial organic carbon (OC) input have increased (Abe et al., 2019; Martens et al., 2022; Meredith et al., 2019; Miller et al., 2010). Additionally, primary production has increased substantially owing to the extended growing season and expanded area of open water. These phenomena are particularly evident in the northern part of the Chukchi

¹ State Key Laboratory of Submarine Geosciences (Hangzhou), Hangzhou 310012, China;

² Second Institute of Oceanography, Ministry of Natural Resources, Hangzhou 310012, China

^{*} Corresponding authors. E-mail: yuxiaoguo@sio.org.cn (YU Xiaoguo). E-mail: zwy885@163.com (ZHANG Weiyan).

Shelf (Ardyna and Arrigo, 2020; Arrigo and van Dijken, 2015; Giesbrecht et al., 2019; Grebmeier et al., 2006; Hill et al., 2018; Lewis et al., 2020). Meanwhile, the volume and velocity of the sediment-laden Pacific inflow have increased obviously (from 0.7×10^6 to 1.2×10^6 m³·s⁻¹) in recent years (Woodgate, 2018). These changes have profound impacts on the carbon cycle that directly affects the air—sea exchange of CO_2 and the organic matter (OM) buried in the sediments. Owing to its high sensitivity to climate change, the Chukchi Shelf is a key region for understanding abrupt climate change based on its past climatic variations.

The Chukchi Sea is characterized by high primary productivity, with export rates averaging 82% (O'Daly et al., 2020). However, a substantial portion of the OC produced or delivered to the region is not buried locally (Astakhov et al., 2013; Bates, 2006; Hill et al., 2018). Based on fatty acid analysis, terrestrial OC (Terr-OC) accounts for 62%, 96%, and 44% of the total buried OC in the sediments of the northern Chukchi Shelf, continental slope, and deep basin, respectively (Belicka and Harvey, 2009; Belicka et al., 2004). These spatial patterns in OC burial underscore source-specific transport dynamics. Moreover, burial dynamics on the northern Chukchi Shelf indicate that marine OC (Mar-OC) undergoes less degradation in the water column prior to burial, resulting in a higher initial burial efficiency than that of Terr-OC (Ye et al., 2024).

The Little Ice Age (LIA), which was a period of widespread cooling that persisted from the early 14th century (end of the Medieval Warm Period) to the mid–late 19th century (onset of the present-day warming trend), was likely the coldest period of the past 8000 a. The beginning and end times of the LIA vary across different regions. The onset of the cooling period in the Arctic Ocean and Europe occurred earlier than in North America, with the coldest period in the Arctic Ocean extending from the 1580s to the mid–late 19th century (Kaufman et al., 2009; Opel et al., 2013; PAGES 2k Consortium, 2013).

Matthes (1939) was the first to refer to the LIA when describing the mountain glacial expansion and retreat in the Sierra Nevada (California, USA) that occurred during the most recent 4000 a. Numerous studies (considering different data sources such as tree rings, fossil soils, and documents with different temporal resolution) have found that the impact of the LIA was regional and that it was not consistently cold throughout the period, i.e., long warm summer periods are known to have occurred (Holzhauser, 2010; Holzhauser et al., 2005; Kaufman et al., 2009; Wanner et al., 2022). As the most recent cold period, internal climatic fluctuation during the LIA has drawn widespread research attention.

Over the past two decades, with the rapid changes in the marine environment, significant progress has been made in reconstructing the Holocene environmental conditions, sea ice fluctuation and OC burial in the northern Chukchi Shelf, particularly north of 73°N (Astakhov et al., 2020; Cooper and Grebmeier, 2018; Polyak et al., 2016; Song et al., 2022; Stein et al., 2017; Yamamoto et al., 2017; Ye et al., 2024). However, the last centuries in these works remain limited.

The objectives of this study were to explore the fluctuation in sea ice during the LIA through investigation of changes in the ice-rafted debris (IRD) content of sediments, and to elucidate the evolution of the content and composition of OM in the sediments under the climate anomaly condition. As the most reliably documented, relatively large climate anomaly of the last millennium (prior to the industrial revolution), understanding the burial of OM in sediment during the LIA is important for comprehension of the natural carbon cycle variability.

2 Samples and methods

2.1 Samples and environmental setting

Sediment core ARC7-R11 (hereafter, R11) was collected from the Chukchi Shelf (73.802°N, 168.968°W; water depth: 155 m) by multicores during the 7th Chinese National Arctic Research Expedition (CHINARE) in summer 2016 (Figure 1). Core R11 (length: 34 cm) was subsampled into 1-cm intervals onboard the Research Vessel *Xuelong* and stored in a freezer at -20 °C prior to analysis.

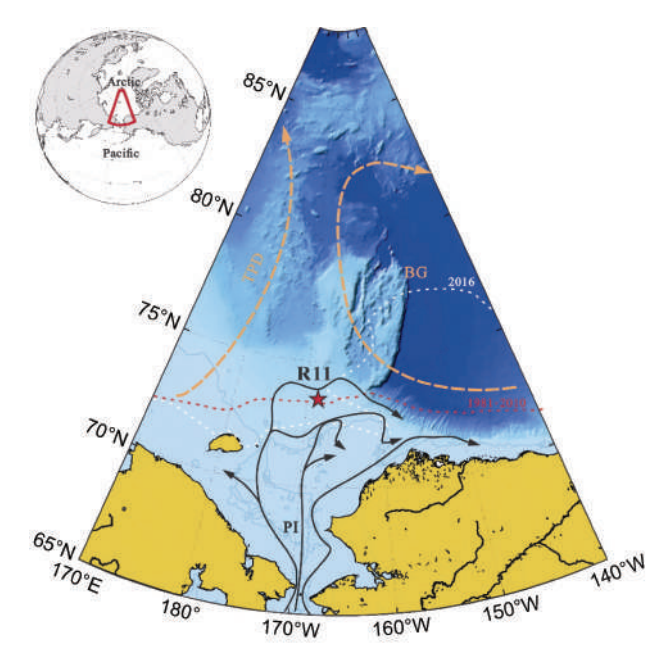


Figure 1 Core R11 (red star) location and surface currents. PI indicates Pacific inflow (Corlett and Pickart, 2017), BG indicates Beaufort Gyre and TPD indicates transpolar drift (Timmermans and Toole, 2023). Red and white dashed lines indicate the sea ice extent minimum (15% ice concentration) for the 30-year period (1981–2010) and for 2016 (Melsheimer and Spreen, 2019), respectively.

The core was obtained in the northern part of the Chukchi Shelf, where the Pacific inflow and bottom flow have low velocity (Coachman and Aagaard, 1966; Darby et al., 2009; Woodgate, 2018), in a region far from the coastal zone and where there is no large riverine input. The sediment grain size is finer in comparison with that in the southern part of the Chukchi Shelf (Gao et al., 2023; Zhang W Y et al., 2018), and both the regional primary productivity and the export of particulate OC to the seabed are higher (Giesbrecht et al., 2019; Hill et al., 2018). Additionally, the permanent sea ice margin is located in this area, meaning that the impact of sea ice retreat resulting from the higher temperatures in recent times can be determined (Tschudi et al., 2019).

Methods

²¹⁰Pb 2.2.1

The ²¹⁰Pb concentrations were measured to determine the chronology of Core R11 using ORTEC HPGe detectors (GEM, Lo-Ax and GMX) at the Nanjing Institute of Geography and Limnology, China, Approximately 10 g of ground dry sediment was passed through a 100-mesh sieve. The resultant material was placed into a tube, which was then sealed and set aside for 20 d before testing.

2.2.2 Grain size and IRD

Grain size and IRD analysis were performed using a Malvern 2000 laser particle size analyzer at the State Key Laboratory of Submarine Geosciences (Hangzhou, China), following the "Specifications for oceanographic survey-Part 8: Marine geology and geophysics survey: GB/T 12763.8—2007" guidelines (National Technical Committe for Marine Standardization, 2007). The range of particle size measurements was 0.02–2000 um, with a relative error of repeated measurements of <3%. Grain size parameters were calculated according to the moment method (McManus, 1988).

2.2.3 Bulk carbon, nitrogen, and stable isotopes

Freeze-dried samples were homogeneously ground using a mortar and pestle and pretreated with 1 mol·L⁻¹HCl to remove carbonate before isotopic analysis.

The total OC (TOC) and total nitrogen (TN) content and their stable isotopic compositions were measured using a Thermo Finnigan Delta plus AD mass spectrometer connected to a Conflo III interfaced with an elemental analyzer (EA112). Reference materials USGS-24, GBW4408, and IAEA-N1 were used to calibrate the pure CO₂ and N₂ from the lab tank. Analytical precision for carbon and nitrogen was within ±0.2% and reproducibility was 20%.

2.2.4 Endmember model

Previous studies have shown that the branched and isoprenoid tetraether index based on glycerol dialkyl glycerol tetraethers in sediments is less than 0.1, indicating a low proportion of soil-derived OM in the study area (Yu et al., 2015; Park et al., 2014). The dual-isotope three-endmember mixing model also suggested the lower proportion of topsoil-OC in the northern part of the Chukchi Shelf (Ren et al., 2025). Therefore, a simplified two-endmember isotopic model was used to estimate the relative percentages of Mar-OC and Terr-OC in the R11 sediment. The fractions of marine- and terrestrially derived OC in the sediments of Core R11 were estimated using the endmember model according to Equations (1)–(3). Considering the δ^{13} C values of OM from the East Siberian ice-complex deposits (-32.1%), topsoil permafrost (-27.5%) (Semiletov et al., 2016; Vonk et al., 2010), and riverine (-27.8%) (Belicka and Harvey, 2009), the end-member value for Terr-OC was selected as -27.1% (Martens et al., 2019; Ye et al., 2024). The marine δ^{13} C end-member depends on the correlation between the Δ^{14} C and δ^{13} C values of sediments in the Chukchi Shelf. The modern fraction (FM) of OM is the ratio between measured Δ^{14} C and the 1950 atmospheric Δ^{14} C. Then, assuming that all OM is derived from modern marine primary production (i.e., FM=100%), the δ^{13} C value for the marine-end member was set as -19.8% (Martens et al., 2019; Ye et al., 2024). Then, the Mar-OC and Terr-OC contents were derived using Equations (4) and (5), respectively:

$$C_{\delta^{13}\text{C_sample}} = f_{\text{marine}} \times C_{\delta^{13}\text{C_marine}} + (1 - f_{\text{marine}}) \times C_{\delta^{13}\text{C terrestrial}}$$
(1)

$$(1-f_{\text{marine}}) \times C_{\delta^{13}\text{C_terrestrial}}$$

$$f_{\text{marine}} = 100 \times (C_{\delta^{13}\text{C_sample}} + C_{\delta^{13}\text{C_terrestrial}}) \times (C_{\delta^{13}\text{C_sample}} + C_{\delta^{13}\text{C_terrestria$$

$$(C_{\delta^{13}\text{C}_marine} + C_{\delta^{13}\text{C}_terrestrial})^{-1}$$
 (2)

$$f_{\text{terrestrial}} = 100 - f_{\text{marine}}$$
(2)

$$C_{\text{Mar-OC}} = f_{\text{marine}} \times C_{\text{TOC}}$$
 (4)

$$C_{\text{Terr-OC}} = f_{\text{terrestrial}} \times C_{\text{TOC}}$$
 (5)

where f_{marine} is the fraction of marine-derived OC (%), $f_{\text{terrestrial}}$ is the fraction of terrestrially derived OC (%), endmember $C_{\delta^{13}\text{C marine}}$ =-19.8‰ Pee Dee Belemnite (PDB), and endmember $C_{\delta^{13}\text{C terrestrial}} = -27.1\%$ PDB (Martens et al., 2022; Ye et al., 2024).

Results

3.1 Sedimentation rate and dating

A sedimentation rate of 0.069 cm·a⁻¹ (n=6, R²=0.7533; Figure 2) for the upper 7 cm of Core R11 was calculated using the constant initial concentration model (Oldfield et al., 1978):

$$S = \lambda H / \ln(A_0 \times A_i^{-1}) \tag{6}$$

where S is the sedimentation rate (cm·a⁻¹); λ is the decay constant of ²¹⁰Pb, i.e., 0.03116 a⁻¹; H is the depth of the sample; and A_0 and A_i represent the ²¹⁰Pb excess at the surface and at depth H, respectively.

This model assumes that the deposition of non-equilibrium 210Pb in the sediments has occurred continuously and uniformly over time, with a constant sedimentation rate (Appleby, 2002).

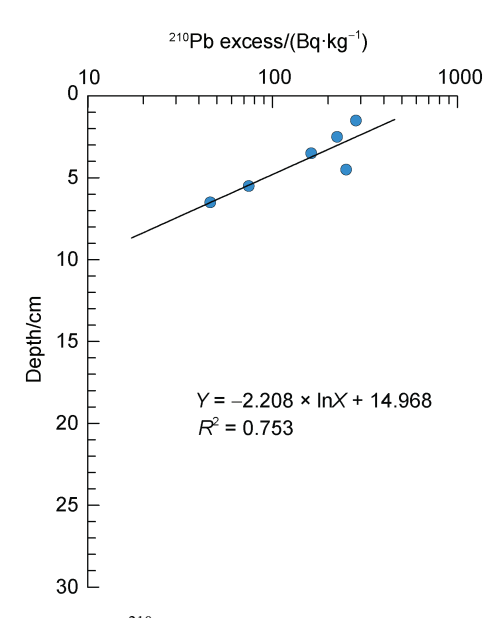


Figure 2 Log of ²¹⁰Pb excess regression relative to sediment depth.

Similar sedimentation rates have been reported for three adjacent stations: H30-11 (72.7411°N, 163.6727°W), 0.1 cm·a⁻¹; HC49-180 (73.3563°N, 175.6230°W), 210 Pb_{ex} 0.06 cm·a⁻¹ and 137 Cs 0.08 cm·a⁻¹ (Cooper and Grebmeier, 2018); ARC6-14R08 (74.0078°N, 168.9750°W), 0.091 cm·a⁻¹ (Astakhov et al., 2019). ASM¹⁴C dating of

mollusk shell fragments from adjacent gravity core sediments (ARC4-R09, 71.96°N, 168.94°W) indicates that the sedimentation rate in the region has been stable from approximately 2800 BP to 2010 (i.e., BC 830–2010) (Song et al., 2022).

Therefore, the uppermost part (1–7 cm) of Core R11 represents sediments accumulated over the past century, while deeper sections were dated using a constant sedimentation rate assumption. The ²¹⁰Pb results indicate that Core R11 comprises approximately a 493-year sediment record (i.e., from 1523 to 2016), covering the LIA and the subsequent period.

3.2 Grain composition and IRD content

The Core R11 sediment is characterized by fine, poorly sorted material comprising mostly silt (43.48%–65.12%. mean: 49.82%) and clay (31.63%–53.92%. mean: 48.78%). Sand components with >2% content occurred at depths of 30–33 cm, 19–22 cm, and 0–5 cm. From the bottom to the top, the silt content increased slightly (Figure 3, Table 1).

Generally, IRD, which is defined as the coarse sediment fraction (>63 μ m, or sometimes even coarser), is used as an indicator of deposition from ice (Polyak et al., 2010). In this study, we defined debris sediment with grain size of >125 μ m as IRD. Thus, it was determined that the IRD content is in the range of 0%–3.47% (mean: 0.54%).

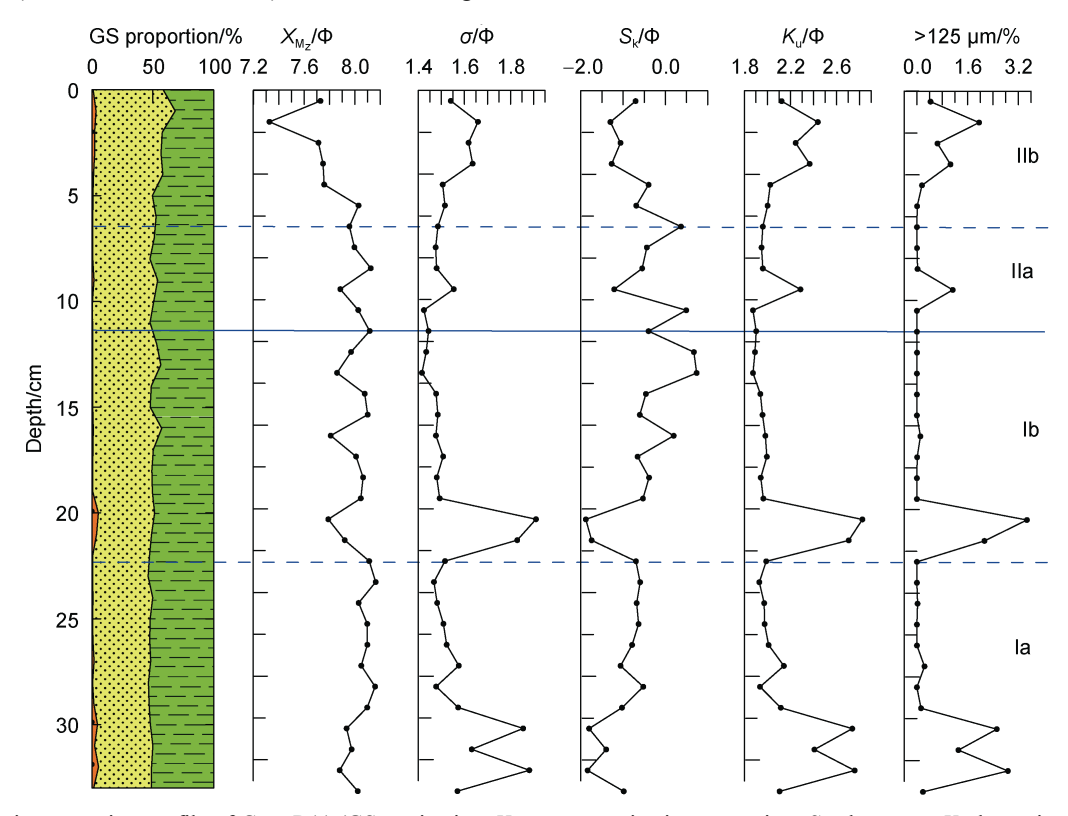


Figure 3 Grain proportion profile of Core R11 (GS, grain size; X_{M_2} , mean grain size; σ, sorting; S_k , skewness; K_u , kurtosis; >125 μm, IRD; green box, clay; yellow box, silt; orange box, sand).

TC . I. I 4	C						
Table 1	Grain	size	composition	and	parameters	ΟĪ	moments

Depth/cm	Gravel/% >2 mm	Sand/% 0.063–2 mm	Silt/% 0.004–0.063 mm	Clay/% <0.004 mm	$X_{ m Mz}/\Phi$	σ/Φ	$S_{\rm k}/\Phi$	$K_{ m u}/\Phi$
0–6	0	1.73	56.46	41.81	7.72	1.58	-0.90	2.20
6-11	0	0.68	49.94	49.38	8.02	1.48	-0.29	1.99
11–22	0	1.36	49.93	48.71	7.99	1.52	-0.39	2.06
22-30	0	0.80	46.69	52.51	8.10	1.52	-0.75	2.01
30-34	0	3.30	45.65	51.05	7.95	1.73	-1.51	2.50

Notes: X_{Mz} indicates mean size; σ indicates sorting index; S_k indicates skewness; K_u indicates kurtosis. Grain size here is reported in the Phi (Φ) scale, where Φ is $-\log_2(\text{diameter in mm})$.

IRD content values >0.5% are found only at depths of 30–33 cm, 20–22 cm, 9–10 cm, and 0–4 cm. In those intervals, the sediments have a higher sorting index (σ) (more poorly sorted) and greater negative skewness values (lower sedimentation energy condition, except for the 0–6-cm interval) compared with the findings in other intervals (Figure 3).

3.3 TOC and TN contents and their isotopic composition

The TOC and TN contents of the sediments are notably higher throughout Core R11 compared with those of the sediments in the southern part of the Chukchi Shelf and other cores collected from adjacent areas (Ren et al., 2025; Zhang W Y et al., 2018).

The TOC content, TN content, and TOC/TN ratio (wt./wt.) are in the range of 1.80%–2.64% (mean: 2.16%), 0.21%–0.33% (mean: 0.24%), and 7.3–11.2 (mean: 9.28), respectively. The δ^{13} C and δ^{15} N values are in the range of –22.59‰ to –21.81‰ (mean: –22.15‰) and 7.99‰–9.42‰ (mean: 8.43‰), respectively.

According to the changes in the TOC content, TN content, δ^{13} C value, δ^{15} N value, and TOC/TN ratio from the bottom to the top, Core R11 was divided into two stages: Stage I (34–12 cm) and Stage II (11–0 cm). Stage I was divided further into two sub-stages: Ia (34–22 cm), with TOC content, TOC/TN ratio, and δ^{13} C values in the range of 2.28%–2.51% (mean: 2.37%), 9.8–11.2 (mean: 10.5), and –22.16‰ to –22.53‰ (mean: –22.29‰), respectively; and Ib (22–12 cm), with TOC content and TOC/TN ratio values showing fluctuating trends of reduction in the range of 1.80%–2.32% (mean: 2.03%), and 8.5–10.1 (mean: 9.4), respectively. Throughout Stage I, the TN content and δ^{15} N values diminished with slight variation in a narrow range, i.e., 0.21%–0.23% (mean: 0.22%) and 7.99‰–8.46‰ (mean: 8.28‰), respectively.

Stage II (11–0 cm) was also divided into two sub-stages: IIa (11–6 cm), with all parameters exhibiting less variation, with TOC and TN contents, the TOC/TN ratio, and δ^{13} C and δ^{15} N values in the range of 1.84%–2.10% (mean: 1.91%), 0.22%–0.23% (mean: 0.23%), 8.0–8.7 (mean: 8.3), -21.93% to -22.19% (mean: -22.06%), and 8.38%–8.51% (mean: 8.44%), respectively; and IIb (6–0 cm), in which the TOC, TN content, and δ^{15} N

values increase markedly in the range of 1.91%-2.64% (mean: 2.25%), 0.24%-0.33% (mean: 0.29%), and 8.67%-9.42% (mean: 8.98%), respectively. The δ^{13} C and TOC/TN ratio values are in the range of -21.81% to -22.11% (mean: -21.99%) and 7.3-8.4 (mean: 7.8), respectively (Figure 4, Table 2).

3.4 Percentage contents of Terr-OC and Mar-OC

The relative percentage contents of Terr-OC and Mar-OC in the sediments of Core R11 were estimated using the endmember model. The fractions of Terr-OC and Mar-OC are in the range of 27.5%–37.4% (mean: 32.2%) and 62.6%–72.5% (mean: 67.8%), respectively. The fraction of Terr-OC is higher at depths of >22 cm (Stage Ia), ranging from 32.3% to 37.4% with a mean value of 34.0%, and it exhibits fluctuating decline toward the top of the core, with the lowest value of 27.5% occurring at the depth of 3 cm. Conversely, Mar-OC exhibits the opposite trend, with the highest fraction in the top 6-cm interval (Stage IIb), ranging from 68.4% to 72.5% with a mean value of 70.1% (Figure 4, Table 2).

4 Discussion

4.1 IRD content reflects sea ice fluctuation

Generally, IRD comprises terrestrial/coastal material transported within a matrix of ice that is deposited in marine sediments when the ice matrix melts (Dowdeswell, 2009). Numerous studies have used IRD as a proxy of glacial/sea ice variability to reconstruct past climate change (Alley and Clark, 1999; Andresen et al., 2012; Darby, 2003, 2008; Darby et al., 2006; Polyak et al., 2016). The presence of IRD in sediments is evidence of the existence of regional seasonal sea ice (sea ice melting in the warmer season). The absence of IRD in sediments can be attributed to two scenarios: either the lack of sea ice development, or the existence of permanent and stable sea ice, preventing debris from being deposited. The former situation is clearly inconsistent with the sea ice conditions of the northern Chukchi Shelf. Therefore, the absence of IRD in the Core R11 sediments implies that perennial sea ice occurred, meaning that the weather was cold.

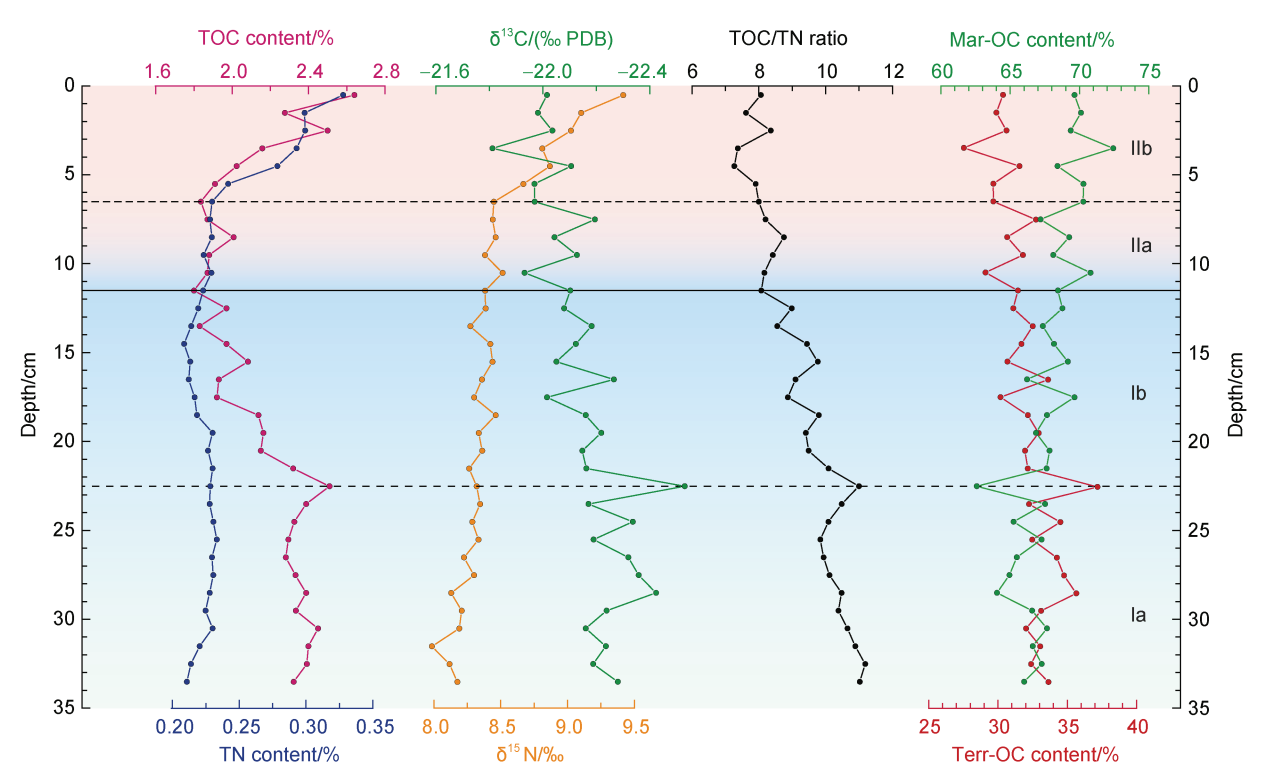


Figure 4 Profiles of TOC content, TN content, δ^{13} C, δ^{15} N, the TOC/TN ratio, and the relative fractions of Mar-OC and Terr-OC.

Table 2 TOC and TN contents and their isotopic composition, and the TOC/TN ratio

Depth/cm TOC conto	TOC content/0/	δ ¹³ C/‰	TN content/%	$\delta^{15}N/\hspace{-0.1cm}\%\hspace{-0.1cm}$	TOC content (wt.)/	Relative fractions		
	TOC content//6	0 C/700			TN content (wt.)	Mar-OC content/%	Terr-OC content/%	
0–6	2.25	-21.99	0.29	8.98	7.8	70.1	29.9	
6-11	1.91	-22.06	0.23	8.44	8.3	68.8	31.2	
11–22	2.03	-22.14	0.22	8.36	9.3	68.0	32.0	
22–34	2.35	-22.29	0.23	8.22	10.5	66.0	34.0	

The distribution of the IRD content in Core R11 shows that there were four warmer intervals, indicating that seasonal sea ice occurred during the 1530s-1580s, 1710s-1730s, 1890s-1900s, and 1980s-2016. The first two intervals suggest that sea ice melting occurred in sub-cold periods during the LIA. The third interval indicates that the sea surface temperature was warmer after the end of the LIA. The final interval is in accord with Modern Warm Period. The IRD content of near zero in the other intervals implies that the area of Core R11 was within the perennial sea ice zone during the 1620s-1700s, 1750s-1880s, and 1900s-1980s. The fluctuation of the sea ice margin of the northern Chukchi Shelf tallies with the retreat and extension of Alpine glaciers which were reconstructed based on historical documents (primarily drawings and paintings) and field discoveries (Wanner et al., 2022; Figure 5), the land-terminating glaciers along the southern coast of Alaska (Barclay et al., 2009a, 2009b, 2013; Solomina et al., 2015), and reconstructions of Alpine and Arctic summer temperature anomalies (Kaufman et al., 2009; Opel et al., 2013; PAGES 2k Consortium et al., 2013; Wanner et al., 2022), and generalized sea-ice histories from Chukchi Sea/Bering Sea based on dinocyst, IP₂₅ and other proxy/records (de Vernal et al., 2008; Leclerc and Halfar, 2024).

The front of perennial sea ice during the Holocene fluctuated approximately along the northern Chukchi Sea (Polyak et al., 2016). The mechanisms behind the rapid northward retreat of sea ice highlight the potential influence of both atmospheric and oceanic processes. Numerous hypotheses have been proposed to explain significant changes, primarily based on:

- a) The strength and position of the Aleutian Low are closely related to the expansion and reduction of sea ice in the Chukchi Sea. A strong, westerly Aleutian Low enhances Pacific inflow, leading to reduced sea ice in the northern of Chukchi Sea (Danielson et al., 2014).
- b) The enhanced positive Arctic Oscillation facilitates northward atmospheric heat transfer from the Bering Sea region, resulting in increased annual melt duration within the Chukchi Sea (Belchansky et al., 2004).

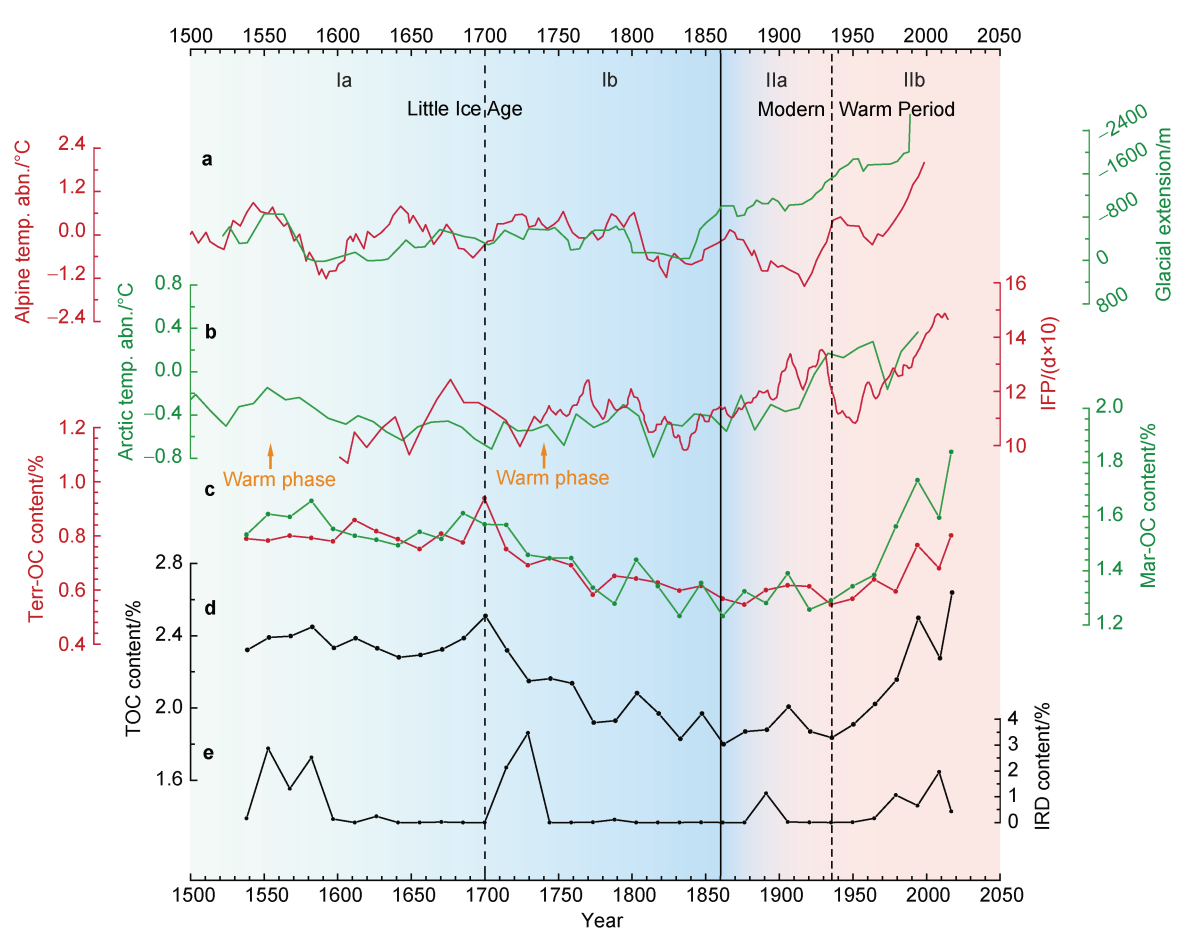


Figure 5 Downcore records of OC content and environmental factors. **a**, Alpine summer temperature anomalies and Alpine Lower Grindelwald Glacier extension (Wanner et al., 2022); **b**, Arctic summer temperature anomalies and ice-free period of the southern Chukchi Shelf (Astakhov et al., 2020; Kaufman et al., 2009); **c**, Terr-OC and Mar-OC contents in sediments; **d**, TOC content in sediments; **e**, IRD content in sediments. IFP indicates ice-free period.

The distribution of IRD in the Core R11 indicated the prevailing role of climate change (manifested by warmer summers) in the variability of ice conditions in the Alaskan–Chukchi sector of the Arctic.

However, the fluctuation of the perennial sea ice margin does not agree with the sea ice extent in the sector of the Barents–Kara seas (Zhang Q et al., 2018), possibly because of the opposing sea ice conditions in eastern and western parts of the Arctic Ocean, that is, ice conditions change differently in different parts of the Eurasian Arctic (Bobylev and Miles, 2020).

4.2 Grain composition and hydrodynamic changes

Hydrodynamic factors play a very important role in the transport and deposition of sediments, directly controlling the type, sorting, distribution, erosion, and deposition of sediments and thereby affecting their spatial distribution. The sediments of Core R11, comprising mainly silt and clay, are finer compared with those of cores obtained in southern parts of the Chukchi Shelf (Zhang W Y et al., 2018). The textural composition and skewness index of the sediments indicate low-energy hydrodynamic conditions during

sedimentation. The sediments on the Chukchi Shelf are compositionally homogeneous, with over 60% of the surface sediment components originating from the Okhotsk-Chukotsk volcanic belt and advected from the Bering Sea (Liu et al., 2023; Viscosi-Shirley et al., 2003). Good correspondence between Chukchi-shelf sediment accumulation patterns and Pacific inflows, which are fairly coherent at all water depths, indicates water circulation is an important sediment transport mechanism in this marginal sea (Viscosi-Shirley et al., 2003). Additionally, the seasonal melting of sea ice releasing the trained sediment, which is also an important source of sediments on the Chukchi Shelf (Darby et al., 2009; Viscosi-Shirley et al., 2003).

Pejrup (1988) established a triangular diagram based on sand, silt, and clay contents to interpret hydrodynamic conditions and to classify the textural composition of the mud fraction ($<4 \, \Phi$) in a recent estuarine environment. The grain composition exhibited a trend of becoming coarser from the bottom to the top, and the content of silt (clay) increased (decreased) gradually. Enhanced hydrodynamics start in the 1830s (depth: 17 cm). After a period of fluctuation from the 1830s to the 1910s (depth: 17 to 8 cm),

it has continued to intensify, especially after the 1940s (top 6 cm) (Figures 3 and 6). This finding is in accord with field observation and the results of previous studies (Myers and Darby, 2022; Woodgate, 2018; Zhang W Y et al., 2018).

Additionally, under cold environmental conditions, the low-energy hydrodynamic condition (Figure 6), poor sorting, and negative skewness parameters also imply that the sand fraction in the intervals with higher sand content (30–34 cm, 20–22 cm and 9–10 cm) originated mainly from sea ice melting.

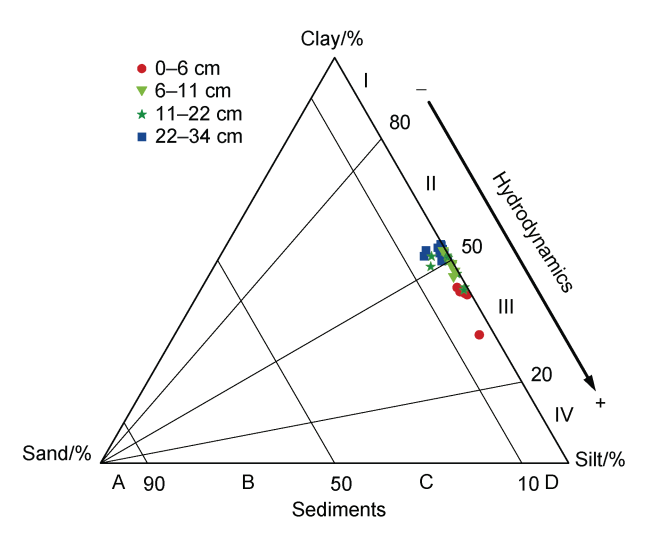


Figure 6 Triangular diagram for hydrodynamic conditions of the depositional environment. Sections I to IV reflect increasingly strong hydrodynamic conditions. The sediments are classified according to their sand content into four sections, A to D (Pejrup, 1988).

4.3 Burial of OM in sediment under climate change

The burial of OM in the sediments is controlled by primary production, transformation processes, and preservation conditions, all of which are sensitive to sea ice fluctuation, sea surface temperature change, and flow hydrodynamics.

To identify the source of the OC in the sediments, the TOC/TN ratios and δ^{13} C values were used as proxies (Bates et al., 2005; Frigstad et al., 2014; Goñi et al., 2019; Meyers et al., 1997; Schubert and Calvert, 2001; Yu et al., 2023; Zhang et al., 2012). Both proxies are sensitive to organism source and are affected by nutrient availability. The composition of OM in the northern part of the Chukchi Shelf is complex, and it includes terrestrial material sourced from coastal erosion, sea ice entrainment, and riverine input, together with material derived from ice algae and plankton (phytoplankton and zooplankton). The content of new riverine carbon is low (<10%) in the sediments of the study area (Ye et al., 2024).

The heavier δ^{13} C PDB values (-22.53% to -21.81%) and medium TOC/TN ratios (7.27-11.18) indicate that the

OM in the sediments is mostly of marine origin. The fractions of Terr-OC and Mar-OC calculated using the endmember model are in the range 27.5%–37.4% (mean: 32.25%) and 62.6%–72.5% (mean: 67.8%), respectively. The values of Terr-OM content and fraction are high between the 1530s and the 1700s, whereas Mar-OC content and fraction exhibit high values starting from the 1940s. High TOC, Terr-OC, and IRD contents reflect sea ice melting and the release of the carried Terr-OC; meanwhile, the marine productivity also increased during the 1530s and the 1700s.

During the LIA and subsequent periods, the content of Mar-OC shows a trend similar to that of the variation in summer temperature anomalies in the Arctic Ocean. In the warmer periods, i.e., the 1520s–1580s and 1940s–2016, temperatures increased and the Mar-OC content also increased; in the cooler period, i.e., 1700s–1860s, temperatures declined and the Mar-OC content also diminished. Meanwhile, Terr-OC correlates with the number of ice-free days in the southern part of the Chukchi Shelf, except for the period 1700s–1880s, during which the Terr-OC content declined continuously despite the number of ice-free days remaining at a high level (Figure 5). This also confirms the contribution of sea ice melting to the Terr-OC component, especially during warmer periods.

High-resolution observations have provided detailed insights into the transport and deposition of particulate OC in the northern Chukchi Sea (Yu et al., 2023). Terr-OC and Mar-OC show pronounced separation within the water column. In particular, lateral transport plays a dominant role in controlling the eventual burial of both Terr-OC and Mar-OC (Xiang and Lam, 2020). Easily resuspendable Terr-OC tends to concentrate within the upper 10 m of the water column or within sea ice and is laterally transported into the deep basin. In contrast, the faster-settling Mar-OC is less influenced by lateral transport and is deposited more directly, extending to the northern Chukchi Shelf margin (Yu et al., 2023).

There has been noticeable change in the characteristics of OM since the 1940s. The contents of TOC and TN, as well as the $\delta^{15}N$ value, have increased continuously, while the fraction of terrestrial OM has shown minor fluctuations around the value of 30% (range: 27.5%–31.6%. mean: 29.9%) (Figures 4–5). This reflects the continuous increase in marine productivity and terrestrial input against the backdrop of global warming.

Concomitantly, the carbon and nitrogen isotope composition of OM in marine plankton is closely related to the utilization of nutrients in water column. Plankton generally preferentially absorb $^{12}\mathrm{C}$ and $^{14}\mathrm{N}.$ Under conditions of nutrient limitation, isotopic fractionation during biological metabolic processes increases leading to higher contents of $^{13}\mathrm{C}$ and $^{15}\mathrm{N}$ in plankton. Increasing $\delta^{15}\mathrm{N}$ values suggest nutrient limitation of phytoplankton growth due to enhanced stratification induced by surface freshening (Bai et al., 2022; Li et al., 2008; Tremblay et al., 2006;

Schubert and Calvert, 2001).

These phenomena are highly comparable to field observations and the findings of recent studies (Ardyna and Arrigo, 2020; Giesbrecht et al., 2019; Hill et al., 2018; Lewis et al., 2020). Under the influence of increased temperature, sea ice retreat increased open water areas and duration of growing season, and promoted productivity (Arrigo and van Dijken, 2015; Kahru et al., 2011). Meanwhile, increased advection of Pacific inflows supplied enough additional nutrients to sustain the higher biomass on the Chukchi Shelf (Lewis et al., 2020). Moreover, they also indicate that the amount of OC buried in sediments is increasing in association with climate warming.

It is interesting that the changes in OM-OC content occur 2–3 decades earlier than those found in IRD and Terr-OC in the downcore records, as exemplified by the marked increase in OM content in the 1680s and 1940s and the subsequent peaks in IRD content in the 1710s and 1970s. The reason for this might reflect the fact that living organisms can quickly react to changes in their environment, whereas the processes of sea ice formation and melting are slower because they depend on the buildup of energy (such as cooling to form ice or warming to melt it) and the achievement of a balance of materials (such as water and salt).

5 Conclusions

Grain size composition (including IRD), OM content, and the isotopic composition of Core R11 (obtained in the northern part of the Chukchi Shelf) record the variation in OC burial and the sedimentation conditions during the LIA and the subsequent period.

The sediment of Core R11 is characterized by fine-grained material (silt and clay components >90%), poor sorting, and high OM content. The deposition conditions were generally characterized by low-energy hydrodynamics, with a trend of enhancement from the bottom upward. The OM originated primarily from marine sources, with terrestrial input of <37.5%. The variation trend of Mar-OC content is similar to that of summer temperature anomalies; as temperature increases, the Mar-OC content also increases, and vice versa. The Terr-OC content correlates with the number of ice-free days in the southern shelf region, except for the period of approximately 1700s to the 1930s.

During warmer periods, seasonal sea ice occurred and the perennial sea ice margin retreated, and the amount of OC buried in the sediments increased. The ability of the sediments to sequester carbon became enhanced, especially after the 1940s.

It is notable that the dating of sediments deeper than 7 cm was based on the assumption of a stable sedimentation rate, which may have limitations.

Acknowledgments This work was financially supported by the National Science Foundation of China (Grant no. 42376064) and the

Chinese Polar Environment Comprehensive Investigation & Assessment Programs (Grant no. CHINARE 2016-03-02). We sincerely appreciate the exceptional support we received from our colleagues during the 7th CHINARE, who assisted us with the field sampling program. The sediment core in this study is provided by Polar Sample Repository, Polar Research Institute of China (http://www.chinare.org.cn/sample). Thanks are extended to 4 anonymous reviewers and Associate Editor Dr. Xuefa Shi for their valuable reviewing comments.

References

- Abe H, Sampei M, Hirawake T, et al. 2019. Sediment-associated phytoplankton release from the seafloor in response to wind-induced barotropic currents in the Bering Strait. Front Mar Sci, 6: 00097, doi: 10.3389/fmars.2019.00097.
- Alley R B, Clark P U. 1999. The deglaciation of the Northern Hemisphere: a global perspective. Annu Rev Earth Planet Sci, 27: 149-182, doi: 10.1146/annurev.earth.27.1.149.
- Andresen C S, Straneo F, Ribergaard M H, et al. 2012. Rapid response of Helheim Glacier in Greenland to climate variability over the past century. Nat Geosci, 5(1): 37-41, doi: 10.1038/ngeo1349.
- Appleby P G. 2002. Chronostratigraphic techniques in recent sediments// Last W M, Smol J P (eds.). Tracking environmental change using lake sediments. Dordrecht: Kluwer Academic Publishers, 171-203, doi: 10.1007/0-306-47669-X 9.
- Ardyna M, Arrigo K R. 2020. Phytoplankton dynamics in a changing Arctic Ocean. Nat Clim Chang, 10: 892-903, doi: 10.1038/s41558-020-0905-y.
- Arrigo K R, van Dijken G L. 2015. Continued increases in Arctic Ocean primary production. Prog Oceanogr, 136: 60-70, doi: 10.1016/j.pocean. 2015.05.002.
- Astakhov A S, Gusev E A, Kolesnik A N, et al. 2013. Conditions of the accumulation of organic matter and metals in the bottom sediments of the Chukchi Sea. Russ Geol Geophys, 54(9): 1056-1070, doi: 10.1016/j.rgg.2013.07.019.
- Astakhov A S, Bosin A A, Liu Y G, et al. 2019. Reconstruction of ice conditions in the northern Chukchi Sea during recent centuries: geochemical proxy compared with observed data. Quat Int, 522: 23-37, doi: 10.1016/j.quaint.2019.05.009.
- Astakhov A S, Shi X F, Darin A V, et al. 2020. Reconstructing ice conditions in the southern Chukchi Sea during the last millennium based on chemical composition of sediments and diatom assemblages. Mar Geol, 427: 106220, doi: 10.1016/j.margeo.2020.106220.
- Bader J, Mesquita M D S, Hodges K I, et al. 2011. A review on Northern Hemisphere sea-ice, storminess and the North Atlantic Oscillation: Observations and projected changes. Atmos Res, 101(4): 809-834, doi: 10.1016/j.atmosres.2011.04.007.
- Bai Y C, Sicre M-A, Ren J, et al. 2022. Centennial-scale variability of sea-ice cover in the Chukchi Sea since AD 1850 based on biomarker reconstruction. Environ Res Lett, 17(4): 044058, doi: 10.1088/1748-9326/ac5f92.
- Barclay D J, Wiles G C, Calkin P E. 2009a. Holocene glacier fluctuations in Alaska. Quat Sci Rev, 28(21/22): 2034-2048, doi: 10.1016/j. quascirev.2009.01.016.
- Barclay D J, Wiles G C, Calkin P E. 2009b. Tree-ring crossdates for a First Millennium AD advance of Tebenkof Glacier, southern Alaska. Quat

- Res, 71(1): 22-26, doi: 10.1016/j.ygres.2008.09.005.
- Barclay D J, Yager E M, Graves J, et al. 2013. Late Holocene glacial history of the Copper River Delta, coastal south-central Alaska, and controls on valley glacier fluctuations. Quat Sci Rev, 81: 74-89, doi: 10.1016/j.quascirev.2013.10.001.
- Bates N R. 2006. Air-sea CO₂ fluxes and the continental shelf pump of carbon in the Chukchi Sea adjacent to the Arctic Ocean. J Geophys Res, 111(C10): C10013, doi: 10.1029/2005JC003083.
- Bates N R, Hansell D A, Bradley Moran S, et al. 2005. Seasonal and spatial distribution of particulate organic matter (POM) in the Chukchi and Beaufort Seas. Deep Sea Res Part II Top Stud Oceanogr, 52(24/26): 3324-3343, doi: 10.1016/j.dsr2.2005.10.003.
- Belchansky G I, Douglas D C, Platonov N G. 2004. Duration of the Arctic sea ice melt season: regional and interannual variability, 1979–2001. J Clim. 17(1): 67-80, doi: 10.1175/1520-0442(2004)017<0067:DOTASI> 2.0.CO;2.
- Belicka L L, Harvey H R. 2009. The sequestration of terrestrial organic carbon in Arctic Ocean sediments: a comparison of methods and implications for regional carbon budgets. Geochim Cosmochim Acta, 73(20): 6231-6248, doi: 10.1016/j.gca.2009.07.020.
- Belicka L L, MacDonald R W, Yunker M B, et al. 2004. The role of depositional regime on carbon transport and preservation in Arctic Ocean sediments. Mar Chem, 86(1/2): 65-88, doi: 10.1016/j.marchem. 2003.12.006.
- Bobylev L P, Miles M W. 2020. Sea ice in the Arctic paleoenvironments// Johannessen O, Bobylev L, Shalina E, et al (eds.). Sea Ice in the Arctic. Cham: Springer, 9-56, doi: 10.1007/978-3-030-21301-5 2.
- Coachman L K, Aagaard K. 1966. On the water exchange through Bering Strait. Limnol Oceanogr, 11(1): 44-59, doi: 10.4319/lo.1966.11.1. 0044.
- Cooper L W, Grebmeier J M. 2018. Deposition patterns on the Chukchi shelf using radionuclide inventories in relation to surface sediment characteristics. Deep Sea Res Part II Top Stud Oceanogr, 152: 48-66, doi: 10.1016/j.dsr2.2018.01.009.
- Corlett W B, Pickart R S. 2017. The Chukchi slope current. Prog Oceanogr, 153: 50-65, doi: 10.1016/j.pocean.2017.04.005.
- Danielson S L, Weingartner T J, Hedstrom K S, et al. 2014. Coupled wind-forced controls of the Bering-Chukchi shelf circulation and the Bering Strait throughflow: Ekman transport, continental shelf waves, and variations of the Pacific-Arctic sea surface height gradient. Prog Oceanogr, 125: 40-61, doi: 10.1016/j.pocean.2014.04.006.
- Darby D A. 2003. Sources of sediment found in sea ice from the western Arctic Ocean, new insights into processes of entrainment and drift patterns. J Geophys Res, 108(C8): 2002JC001350, doi: 10.1029/ 2002jc001350.
- Darby D A. 2008. Arctic perennial ice cover over the last 14 million years. Paleoceanography, 23(1): PA1S07, doi: 10.1029/2007pa001479.
- Darby D A, Polyak L, Bauch H A. 2006. Past glacial and interglacial conditions in the Arctic Ocean and marginal seas—a review. Prog Oceanogr, 71(2/4): 129-144, doi: 10.1016/j.pocean.2006.09.009.
- Darby D A, Ortiz J, Polyak L, et al. 2009. The role of currents and sea ice in both slowly deposited central Arctic and rapidly deposited Chukchi–Alaskan margin sediments. Glob Planet Change, 68(1/2): 58-72, doi: 10.1016/j.gloplacha.2009.02.007.
- de Vernal A, Hillaire-Marcel C, Solignac S, et al. 2008. Reconstructing sea ice conditions in the Arctic and sub-Arctic prior to human

- observations//DeWeaver E T, Bitz C M, Tremblay L B (eds.). Arctic sea ice decline: observations, projections, mechanisms, and implications (Geophysical monograph series). Washington D.C.: American Geophysical Union, 27-45, doi: 10.1029/180GM04.
- Dowdeswell J A. 2009. Ice-rafted debris (IRD)//Gornitz V (ed.). Encyclopedia of paleoclimatology and ancient environments. Dordrecht: Springer, 471-473, doi: 10.1007/978-1-4020-4411-3 113.
- Frigstad H, Andersen T, Bellerby R G J, et al. 2014. Variation in the seston C: N ratio of the Arctic Ocean and pan-Arctic shelves. J Mar Syst, 129: 214-223, doi: 10.1016/j.jmarsys.2013.06.004.
- Gao C, Ruan X Y, Zhang Y G, et al. 2023. Biomarker evidence of the water mass structure and primary productivity changes in the Chukchi Sea over the past 70 years. Front Mar Sci, 10: 1077656, doi: 10.3389/fmars.2023.1077656.
- Giesbrecht K E, Varela D E, Wiktor J, et al. 2019. A decade of summertime measurements of phytoplankton biomass, productivity and assemblage composition in the Pacific Arctic Region from 2006 to 2016. Deep Sea Res Part II Top Stud Oceanogr, 162: 93-113, doi: 10.1016/j.dsr2.2018.06.010.
- Goñi M A, Corvi E R, Welch K A, et al. 2019. Particulate organic matter distributions in surface waters of the Pacific Arctic shelf during the late summer and fall season. Mar Chem, 211: 75-93, doi: 10.1016/j. marchem.2019.03.010.
- Grebmeier J M, Cooper L W, Feder H M, et al. 2006. Ecosystem dynamics of the Pacific-influenced northern Bering and Chukchi Seas in the Amerasian Arctic. Prog Oceanogr, 71(2/4): 331-361. doi: 10.1016/j.pocean.2006.10.001.
- Hill V, Ardyna M, Lee S H, et al. 2018. Decadal trends in phytoplankton production in the Pacific Arctic Region from 1950 to 2012. Deep Sea Res Part II Top Stud Oceanogr, 152: 82-94, doi: 10.1016/j.dsr2.2016.12.015.
- Holzhauser H. 2010. Zur Geschichte des Gornergletschers: ein Puzzle aus historischen Dokumenten und fossilen Hölzern aus dem Gletschervorfeld. Bern: Geographical Institute of the University of Bern, 1-253 (in German).
- Holzhauser H, Magny M, Zumbuühl H J. 2005. Glacier and lake-level variations in west-central Europe over the last 3500 years. Holocene, 15(6): 789-801, doi: 10.1191/0959683605hl853ra.
- Kahru M, Brotas V, Manzano-Sarabio M, et al. 2011. Are phytoplankton blooms occurring earlier in the Arctic? Glob Change Biol, 17(4): 1733-1739, doi: 10.1111/j.1365-2486.2010.02312.x.
- Kaufman D S, Schneider D P, McKay N P, et al. 2009. Recent warming reverses long-term Arctic cooling. Science, 325(5945): 1236-1239, doi: 10.1126/science.1173983.
- Leclerc N, Halfar J. 2024. Review of Arctic sea-ice records over the last millennium from modern, historical, and proxy data sources. Arctic Antarct Alp Res, 56(1): 2392411, doi: 10.1080/15230430.2024. 2392411
- Lewis K M, van Dijken G L, Arrigo K R. 2020. Changes in phytoplankton concentration, not sea ice, now drive increased Arctic Ocean primary production. Science, 369(6500): 198-202, doi: 10.1126/science. aay8380.
- Li H L, Chen J F, Jin H Y, et al. 2008. Biogenic constituents of surface sediments in the Chukchi Sea: implications for organic carbon burying efficiency. Acta Oceanol Sin, 30(1): 165-171 (in Chinese with English abstract).

- Liu Y G, Ren P, Song T F, et al. 2023. Pacific Water impacts the burial of black and total organic carbon on the Chukchi Sea shelf, Arctic Ocean. Palaeogeogr Palaeoclimatol Palaeoecol, 621: 111575, doi: 10.1016/j. palaeo.2023.111575.
- McManus J. 1988. Grain-size determination and interpretation//Tucker M (ed.). Techniques in sedimentology. Oxford: Blackwell, 63-85.
- Martens J, Wild B, Pearce C, et al. 2019. Remobilization of old permafrost carbon to Chukchi Sea sediments during the end of the last deglaciation. Glob Biogeochem Cycles, 33(1): 2-14, doi: 10.1029/2018gb005969.
- Martens J, Wild B, Semiletov I, et al. 2022. Circum-Arctic release of terrestrial carbon varies between regions and sources. Nat Commun, 13(1): 5858, doi: 10.1038/s41467-022-33541-0.
- Matthes F E. 1939. Report of the committee on glaciers, April 1939. Eos Trans Am Geophys Union, 20(4): 518-523, doi:10.1029/TR020i004p00518.
- Melsheimer C, Spreen G. 2019. AMSR2 ASI sea ice concentration data, Antarctic, version 5.4 (NetCDF) (July 2012–December 2019). PANGAEA, doi: 10.1594/PANGAEA.898400.
- Meredith M, Sommerkorn M, Cassotta S, et al. 2019. Polar regions//Pörtner H-O, Roberts D C, Masson-Delmotte V, et al (eds.). The ocean and cryosphere in a changing climate: special report of the Intergovernmental Panel on Climate Change. Cambridge: Cambridge University Press, 203-320.
- Meyers P A. 1997. Organic geochemical proxies of paleoceanographic, paleolimnologic, and paleoclimatic processes. Org Geochem, 27(5/6): 213-250, doi: 10.1016/S0146-6380(97)00049-1.
- Miller G H, Alley R B, Brigham-Grette J, et al. 2010. Arctic amplification: can the past constrain the future? Quat Sci Rev, 29(15/16): 1779-1790, doi: 10.1016/j.quascirev.2010.02.008.
- Myers W B, Darby D A. 2022. A compilation of the silt and clay mineralogy from coastal and shelf regions of the Arctic Ocean. Mar Geol, 454: 106948, doi: 10.1016/j.margeo.2022.106948.
- National Technical Committe for Marine Standardization. 2007. Specifications for oceanographic survey—Part 8: Marine geology and geophysics survey: GB/T 12763.8—2007. Beijing: Standards Press of China (in Chinese).
- O'Daly S H, Danielson S L, Hardy S M, et al. 2020. Extraordinary carbon fluxes on the shallow Pacific Arctic shelf during a remarkably warm and low sea ice period. Front Mar Sci, 7: 548931, doi: 10.3389/fmars. 2020.548931.
- Oldfield F, Appleby P G, Battarbee R W. 1978. Alternative ²¹⁰Pb dating: results from the new Guinea Highlands and lough erne. Nature, 271(5643): 339-342, doi: 10.1038/271339a0.
- Opel T, Fritzsche D, Meyer H. 2013. Eurasian Arctic climate over the past millennium as recorded in the Akademii Nauk ice core (Severnaya Zemlya). Clim Past, 9(5): 2379-2389, doi: 10.5194/cp-9-2379-2013.
- PAGES 2k Consortium. 2013. Continental-scale temperature variability during the past two millennia, Nat Geosci, 6: 339-346, doi: 10.1038/ngeo1797.
- Park Y-H, Yamamoto M, Nam S-I, et al. 2014. Distribution, source and transportation of glycerol dialkyl glycerol tetraethers in surface sediments from the western Arctic Ocean and the northern Bering Sea. Mar Chem, 165: 10-24, doi: 10.1016/j.marchem.2014.07.001.
- Pejrup M. 1988. The triangular diagram used for classification of estuarine sediments: a new approach//de Boer P L, van Gelder A, Nio S D (eds.).

- Tide-influenced sedimentary environments and facies. Dordrecht: Reidel, 289-300, doi: 10.1007/978-94-015-7762-5 21.
- Polyak L, Alley R B, Andrews J T, et al. 2010. History of sea ice in the Arctic. Quat Sci Rev, 29(15/16): 1757-1778, doi: 10.1016/j.quascirev. 2010.02.010.
- Polyak L, Belt S T, Cabedo-Sanz P, et al. 2016. Holocene sea-ice conditions and circulation at the Chukchi-Alaskan margin, Arctic Ocean, inferred from biomarker proxies. Holocene, 26(11): 1810-1821, doi: 10.1177/0959683616645939.
- Ren P, Hillaire-Marcel C, Wang M M, et al. 2025. Sources, transport, age, and evolution of terrestrial organic carbon across the Chukchi Sea margin, Arctic Ocean. Glob Planet Change, 253: 104978, doi: 10.1016/j.gloplacha.2025.104978.
- Schubert C J, Calvert S E. 2001. Nitrogen and carbon isotopic composition of marine and terrestrial organic matter in Arctic Ocean sediments: implications for nutrient utilization and organic matter composition. Deep Sea Res Part I Oceanogr Res Pap, 48(3): 789-810, doi: 10.1016/S0967-0637(00)00069-8.
- Semiletov I, Pipko I, Gustafsson ö, et al. 2016. Acidification of East Siberian Arctic Shelf waters through addition of freshwater and terrestrial carbon. Nat Geosci, 9: 361-365, doi: 10.1038/ngeo2695.
- Solomina O N, Bradley R S, Hodgson D A, et al. 2015. Holocene glacier fluctuations. Quat Sci Rev, 111: 9-34, doi: 10.1016/j.quascirev.2014. 11.018
- Song T F, Hillaire-Marcel C, de Vernal A, et al. 2022. A reassessment of Nd-isotopes and clay minerals as tracers of the Holocene Pacific water flux through Bering Strait. Mar Geol, 443: 106698, doi: 10.1016/i.margeo.2021.106698.
- Stein R, Fahl K, Schade I, et al. 2017. Holocene variability in sea ice cover, primary production, and Pacific-Water inflow and climate change in the Chukchi and East Siberian Seas (Arctic Ocean). J Quat Sci, 32(3): 362-379. doi:10.1002/jgs.2929.
- Timmermans M L, Toole J M. 2023. The Arctic Ocean's Beaufort Gyre. Annu Rev Mar Sci, 15: 223-248, doi: 10.1146/annurev-marine-032122-012034.
- Tremblay J É, Michel C, Hobson K A, et al. 2006. Bloom dynamics in early opening waters of the Arctic Ocean. Limnol Oceanogr, 51(2): 900-912, doi: 10.4319/lo.2006.51.2.0900.
- Tschudi M, Meier W N, Stewart J S, et al. 2019. EASE-grid sea ice age (NSIDC-0611, version 4). Boulder: NASA National Snow and Ice Data Center Distributed Active Archive Center, doi: 10.5067/UTAV7490FEPB.
- Viscosi-Shirley C, Pisias N, Mammone K. 2003. Sediment source strength, transport pathways and accumulation patterns on the Siberian–Arctic's Chukchi and Laptev shelves. Cont Shelf Res, 23(11/13): 1201-1225, doi: 10.1016/S0278-4343(03)00090-6.
- Vonk J E, Sánchez-García L, Semiletov I, et al. 2010. Molecular and radiocarbon constraints on sources and degradation of terrestrial organic carbon along the Kolyma paleoriver transect, East Siberian Sea. Biogeosciences, 7: 3153-3166, doi: 10.5194/bg-7-3153-2010.
- Wanner H, Pfister C, Neukom R. 2022. The variable European Little Ice Age. Quat Sci Rev, 287: 107531, doi: 10.1016/j.quascirev.2022.107531.
- Woodgate R A. 2018. Increases in the Pacific inflow to the Arctic from 1990 to 2015, and insights into seasonal trends and driving mechanisms from year-round Bering Strait mooring data. Prog Oceanogr, 160: 124-154, doi: 10.1016/j.pocean.2017.12.007.

- Woodgate R A, Weingartner T, Lindsay R. 2010. The 2007 Bering Strait oceanic heat flux and anomalous Arctic sea-ice retreat. Geophys Res Lett, 37(1): 2009GL041621, doi: 10.1029/2009gl041621.
- Xiang Y, Lam P J. 2020. Size-fractionated compositions of marine suspended particles in the western Arctic Ocean: lateral and vertical sources. J Geophys Res Oceans, 125(8): e2020JC016144, doi: 10.1029/2020JC016144.
- Yamamoto M, Nam S-I, Polyak L, et al. 2017. Holocene dynamics in the Bering Strait inflow to the Arctic and the Beaufort Gyre circulation based on sedimentary records from the Chukchi Sea. Clim Past, 13(9): 1111-1127, doi: 10.5194/cp-13-1111-2017.
- Ye L M, Yu X G, Liu Y G, et al. 2024. Organic carbon burial dynamics at the Chukchi Shelf margin: implications for the Arctic Ocean carbon sink. Palaeogeogr Palaeoclimatol Palaeoecol, 655: 112534, doi: 10.1016/j.palaeo.2024.112534.
- Yu X G, Bian Y P, Ruan X Y, et al. 2015. Glycerol dialkyl glyceroltetraethers and Tex₈₆ index in surface sediments of the Arctic

- Ocean and the Bering Sea. Mar Geol Quat Geol, 35(3): 11-22 (in Chinese with English abstract).
- Yu X G, Ye L M, Bian Y P, et al. 2023. Composition and sources of suspended particles in the Pacific Arctic region. Mar Environ Res, 191: 106127, doi: 10.1016/j.marenvres.2023.106127.
- Zhang R, Chen M, Guo L D, et al. 2012. Variations in the isotopic composition of particulate organic carbon and their relation with carbon dynamics in the western Arctic Ocean. Deep Sea Res Part II Top Stud Oceanogr, 81-84: 72-78, doi: 10.1016/j.dsr2.2011.05.005.
- Zhang Q, Xiao C D, Ding M H, et al. 2018. Reconstruction of autumn sea ice extent changes since AD1289 in the Barents-Kara Sea, Arctic. Sci China Earth Sci, 61(9): 1279-1291, doi: 10.1007/s11430-017-9196-4.
- Zhang W Y, Yu X G, Wang W G, et al. 2018. Records of organic carbon and total nitrogen for environmental changes in the Chukchi Sea during the past 100 years. Mar Geol Quat Geol, 38(2): 13-24, doi: 10.16562/j.cnki.0256-1492.2018.02.002 (in Chinese with English abstract).